Resilience Assessment of Interdependent Energy Systems Under Hurricanes

Huajun Zhang, *Student Member, IEEE*, Peng Wang, *Fellow, IEEE*, Shuhan Yao, *Student Member, IEEE*, Xiaochuan Liu, *Student Member, IEEE*, and Tianyang Zhao, *Member, IEEE*

***Abstract*—Energy systems, e.g., power systems and natural gas systems, are increasingly interdependent, which brings benefits under normal conditions and introduces risks under extreme weather events, e.g., hurricanes. A comprehensive method is proposed to reflect the spatial-temporal hurricane impacts on interdependent power and natural gas systems. Mechanism analysis based and data based component failure models are used to map hurricane effects on exposed component failure probabilities based on which system states are generated using Monte Carlo simulation. For system states with failed components, the integrated energy flow is developed to determine minimum joint load shedding considering inherent properties of each system and characteristics of interdependence coordinately. Operational metrics and infrastructure metrics are employed to quantify the service adequacy and network resistance of the interdependent energy systems, respectively. The modified IEEE 24-reliability test system and the 12-node natural gas system under a simulated hurricane are used to validate the effectiveness of the proposed method. Simulation results show the method can identify weak parts and quantify the performance of interdependent power and natural gas systems under hurricanes to provide information for effective and coordinative preparedness.**

***Index Terms*—hurricane, interdependence, component failure, resilience, integrated energy flow.**

I. Introduction

ALONG THE EVOLUTION of energy systems, power systems and natural gas (NG) systems have become highly interdependent due to the increasing connections among them. For example, the utilization of NG for power generation has grown steadily [1] while gas facilities are also preferably driven by electricity [2]. Interdependence provides environmental, economic, and operational benefits under normal conditions [3], [4]. However, risks associated with interdependence might emerge under extreme weather events (EWEs) [5]. Mitigating the threats from EWEs, resilience-oriented research on energy systems has gained growing attention from independent systems to interdependent ones.

The resilience of a system under EWEs is directly associated to the system features and characteristics of the extreme event it suffers [6]. In the area of power system, various works have been done in components failure models under EWEs, resilience assessment methods, resilience metrics as well as resilience enhancement strategies. Under EWEs, the failure probability of exposed components, e.g., power transmission towers, is closely related to the evolving weather conditions. Traditional models, e.g., the two or multi-state weather models [7] as well as the regional weather model [8] are not adequate to capture the impact of time-space-changing weather conditions on component failure probabilities. Statistical models based on data [9], [10] and models based on mechanism analysis [11], [12] represent component failure as functions of various factors, and take continuously changing weather condition as an input variable, thus can better reflect the weather impact on component failure probabilities from both spatial and temporal perspectives. [13] develops a conceptual framework to provide fundamentals to model and quantify the power system resilience. [14] presents a probabilistic method to evaluate the resilience of power distribution systems under different weather scenarios. [15], [16] propose resilience metrics from different perspectives, e.g., operation, infrastructure, and topology etc., to quantify the power system resilience specifically. [17], [18] introduce resilience enhancement strategies.

Coordination of interdependent power and NG systems under normal conditions has been well studied in e.g., co-optimal planning [19], optimal energy flow [20], and operation scheduling [3], [4], to utilize interdependence to achieve benefits. Under EWEs, interdependence could introduce risks as disruptions in one system can permeate to the connected ones and may loop back through coupling links. For example, quit of gas compressors due to electricity cut off caused by EWEs may result in gas load shedding, which could lead to fuel reduction even interruption supplied to gas-fired generators (GFGs). A shortage of fuel could further contribute to the outage in the power system. However, little work is done to explore the performance of interdependent power and NG systems under EWEs considering individual system properties and interdependence characteristics coordinately. [21] proposes a proactive method to

Manuscript received July 1, 2019; revised October 31, 2019; accepted February 8, 2020. Date of publication February 13, 2020; date of current version August 24, 2020. This work was supported by the Future Resilient System at the Singapore-ETH Centre funded by the National Research Foundation of Singapore (NRF) under its Campus for Research Excellence and Technological Enterprise program. Paper no. TPWRS-00934-2019. *(Corresponding author: Tianyang Zhao.)*

Huajun Zhang and Shuhan Yao are with the Interdisciplinary Graduate School, Nanyang Technological University, Singapore 639798, Singapore (e-mail: hzhang031@e.ntu.edu.sg; syao002@e.ntu.edu.sg).

Peng Wang and Xiaochuan Liu are with the School of Electrical and Electronic Engineering, Nanyang Technological University, Singapore 639798, Singapore (e-mail: epwang@ntu.edu.sg; e160064@e.ntu.edu.sg).

Tianyang Zhao is with the Energy Research Institute@NTU, Nanyang Technological University, Singapore 639798, Singapore (e-mail: zhaoty@ntu.edu.sg).

Color versions of one or more of the figures in this article are available online at http://ieeexplore.ieee.org.

Digital Object Identifier 10.1109/TPWRS.2020.2973699

enhance the preparedness of multiple energy carrier microgrids by energy storage, using steady-state gas flow model without modeling compressors. [22] proposes a resilience-constrained unit commitment model to enhance the resilience of the integrated power distribution and NG system without modeling the hurricane impact on component failures directly. The background highlights the necessity to investigate, understand, model, and quantify the performance of interdependent power and NG systems under EWEs for coordinative and proactive preparedness.

Under this background, this paper proposes a comprehensive method to quantify the performance of interdependent power and NG systems under hurricanes. Mechanism analysis based and data based component failure models are used to reflect hurricane effects on the component failure probabilities, which are input to the Monte Carlo simulation to simulate component states. When components are simulated to fail, integrated energy flow is developed to determine the optimal joint load shedding over time. Operational and infrastructure indices are used to describe the performance of the interdependent systems. The contribution of this paper can be summarized as follows: 1) Develop a method that evaluates hurricane impacts on the performance of interdependent power and NG systems. 2) Propose the integrated energy flow taking into account individual system properties and interface characteristics to minimize the joint load shedding. 3) Integrate operational and infrastructure indices to quantify the performance of interdependent systems.

The remainder of this paper is divided into five sections. Section II introduces component failure models under hurricanes. Section III models interdependent energy systems. Section IV presents the resilience assessment method and indices. Section V conducts case studies. Section VI concludes.

II. Component Failure Models Under Hurricanes

Under hurricanes, some components, e.g., transmission towers and conductors are directly exposed to the hurricane wind and rainfall, while some are not, e.g., components underground and shielded in buildings. In this work, the hurricane impact caused by intense wind and strong rainfall is considered, while the flood effect is not included. Thus, the failures of underground gas components under hurricanes, which are mainly related to the flood are not taken into account in this paper. This section maps hurricane impacts on failure probabilities of exposed transmission towers and conductors, using mechanism analysis based and data based models, respectively. The assessment horizon $\mathcal{T}$ is divided into equal time intervals with a length of $\Delta t = 1$ h, and $T = |\mathcal{T}|$.

A. Failure Model of Power Transmission Towers

The effect of hurricanes on a tower is closely related to the tower responses based on its structural characteristics. The fragility curve is used to work out the probability of tower failure under hurricanes. The fragility curve describes the damage probability of a component as the function of the extreme weather factors, such as the hurricane wind.

In addition to strong wind, hurricanes also introduce heavy rain. The rainfall impact is taken into account through the concept of equivalent wind speed, as introduced in [23], as follows:

$$\mathcal{V}^{*t}_{\mathrm{tw},k} = \mathcal{V}^{t}_{\mathrm{tw},k} + a_{\mathrm{tw}}(Rf^{t}_{\mathrm{tw},k})^{b_{\mathrm{tw}}}\exp(c_{\mathrm{tw}}\mathcal{V}^{t}_{\mathrm{tw},k}) - d_{\mathrm{tw}}\exp(e_{\mathrm{tw}}\mathcal{V}^{t}_{\mathrm{tw},k}),\ \forall t\in\mathcal{T}, k\in\mathcal{E}_{\mathrm{tw}} \quad (1)$$

where the term $\mathcal{V}^{t}_{\mathrm{tw},k}$ ($\mathrm{m\cdot s^{-1}}$) is the 3-second, 10-meter wind speed[1] at the location of tower k. $Rf^{t}_{\mathrm{tw},k}$ ($\mathrm{mm}\cdot h^{-1}$) is the rainfall rate at the tower site. $\mathcal{V}^{*t}_{\mathrm{tw},k}$ ($\mathrm{m}\cdot s^{-1}$) is the equivalent wind speed. a_{tw}, b_{tw}, c_{tw}, d_{tw} and e_{tw} are constants. $\mathcal{E}_{\mathrm{tw}}$ is the set of transmission towers.

The failure probability $\pi^{t}_{\mathrm{tw},k}$ of tower k can be mathematically described by the lognormal fragility curve [24] as follows:

$$\pi^{t}_{\mathrm{tw},k} = \frac{1}{\sqrt{2\pi}\alpha_{\mathrm{tw},k}}\int_{-\infty}^{x^{t}_{\mathrm{tw},k}}\exp\left(\frac{-(\tau-\mu^{t}_{\mathrm{tw},k})^2}{2(\alpha_{\mathrm{tw},k})^2}\right)d\tau,\quad \forall t\in\mathcal{T}, k\in\mathcal{E}_{\mathrm{tw}} \quad (2)$$

where $x^{t}_{\mathrm{tw},k} = \ln\mathcal{V}^{*t}_{\mathrm{tw},k}$. $\mu_{\mathrm{tw},k}$ and $\sigma_{\mathrm{tw},k}$ are the logarithmic mean and standard deviation, respectively.

The attacking angle of hurricane wind on towers also has an impact on the tower failure probability. Various of $\mu_{\mathrm{tw},k}$ and $\sigma_{\mathrm{tw},k}$ in (2) are used to reflect the influence of wind attacking angle [23].

B. Failure Model of Power Transmission Conductors

The regression model proposed in [25] is extended to take into account rainfall impact in addition to strong wind. The transmission conductor is divided into appropriate number of equal segments, each of which is assumed to be with the same terrain features and exposed to the hurricane intensity at the central location of each segment. The time-varying failure rate $\lambda^{t}_{\mathrm{cs},k}$ (faliure $\cdot$ $\mathrm{km^{-1}}\cdot$ $\mathrm{h^{-1}}$) of conductor segment k at time slot t is expressed as follows:

$$\lambda^{t}_{\mathrm{cs},k} = L_{\mathrm{cs},k}\exp\left(\frac{a_{\mathrm{cs},k}\mathcal{V}^{t}_{\mathrm{cs},k}}{\mathcal{V}_{\mathrm{dcs},k}} + \frac{b_{\mathrm{cs},k}Rf^{t}_{\mathrm{cs},k}}{Rf_{\mathrm{dcs},k}} + c_{\mathrm{cs},k}\right),\quad \forall t\in\mathcal{T}, k\in\mathcal{E}_{\mathrm{cs}} \quad (3)$$

where $L_{\mathrm{cs},k}$ (km) is the segment length. $\mathcal{V}^{t}_{\mathrm{cs},k}$ ($\mathrm{m\cdot s^{-1}}$) and $Rf^{t}_{\mathrm{cs},k}$ ($\mathrm{mm\cdot h^{-1}}$) are the wind speed and rainfall rate at the location of segment k, respectively. $\mathcal{V}_{\mathrm{dcs},k}$ ($\mathrm{m\cdot s^{-1}}$) and $Rf_{\mathrm{dcs},k}$ ($\mathrm{mm\cdot h^{-1}}$) are the design value of wind speed and rainfall rate for segment k, respectively. $a_{\mathrm{cs},k}$, $b_{\mathrm{cs},k}$, and $c_{\mathrm{cs},k}$ are parameters derived from historical data. $\mathcal{E}_{\mathrm{cs}}$ is the set of transmission conductor segments.

Then, without considering repairs, according to the discrete-time Markov process with constant failure rate at time slot t, the failure probability $\pi^{t}_{\mathrm{cs},k}$ of segment k is calculated as follows [26]:

$$\pi^{t}_{\mathrm{cs},k} = (1-\pi^{t\text{-}1}_{\mathrm{cs},k})(1-\exp(-\lambda^{t}_{\mathrm{cs},k}\cdot t)) + \pi^{t\text{-}1}_{\mathrm{cs},k},\quad \forall t\in\mathcal{T}, k\in\mathcal{E}_{\mathrm{cs}} \quad (4)$$

[1]Wind speed in the remaining part of this paper refers to 3-second gust at 10 m height.

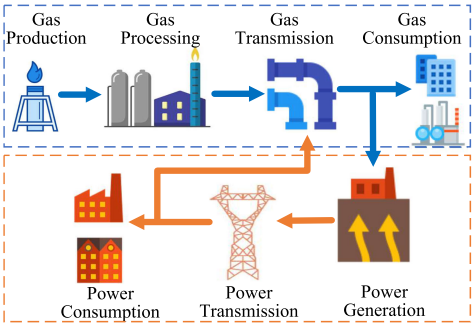

Fig. 1. Interdependent power system and NG systems.

III. Interdependent Energy System Models

The interdependent power system and NG system are physically connected as shown in Fig. 1 through GFGs and gas compressors driven by electricity. When exposed transmission towers or conductors failed under hurricanes, disruptions in the power system may permeate to the NG system and further loop back. To sufficiently explore the behavior of the interdependent power and NG systems with components failures caused by hurricanes, inherent properties of each system and interdependence characteristics need to be modeled coordinately.

A. Power System Model

After generation, the power is transmitted to substations through transmission networks consisting of branches, circuit breakers, switches, etc. Considering the status, the real-time generator output constraints are given as follows:

$$p^t_{\mathrm{e},g} - p^{t\text{-}1}_{\mathrm{e},g} \le R^{60+}_{\mathrm{e},g} \cdot tu^t_{\mathrm{e},g},\ \forall t \in \mathcal{T}, g \in \mathcal{G} \tag{5}$$

$$p^{t\text{-}1}_{\mathrm{e},g} - p^t_{\mathrm{e},g} \le R^{60\text{-}}_{\mathrm{e},g} \cdot tu^{t\text{-}1}_{\mathrm{e},g},\ \forall t \in \mathcal{T}, g \in \mathcal{G} \tag{6}$$

$$P^t_{\mathrm{e},g} - R^t_{\mathrm{e},g} \le p^t_{\mathrm{e},g} \le P^t_{\mathrm{e},g} + R^t_{\mathrm{e},g}, \forall t \in \mathcal{T}, g \in \mathcal{G} \tag{7}$$

where $\mathcal{G}$ is the set of generators. $R^{60+}_{\mathrm{e},g}$ (MW·h^{-1}) and $R^{60\text{-}}_{\mathrm{e},g}$ (MW·h^{-1}) are the maximum 60-min ramp-up and ramp-down rate of unit g. $p^t_{\mathrm{e},g}$ (MW) is the active power output of generator g. $u^t_{\mathrm{e},g}$ is the on ($u^t_{\mathrm{e},g} = 1$) / off ($u^t_{\mathrm{e},g} = 0$) status of unit g. $P^t_{\mathrm{e},g}$ (MW) is the set-point of unit g during time slot t. $R^t_{\mathrm{e},g}(MW)$ is the reserve capacity of unit g. $u^t_{\mathrm{e},g}$, $P^t_{\mathrm{e},g}$ and $P^t_{\mathrm{e},g}$ are first stage decision variables determined by the two-stage robust unit commitment model for integrated energy systems as described in Appendix. $P^{\min}_{\mathrm{e},g}$ (MW) and $P^{\max}_{\mathrm{e},g}$(MW) are the low and up bound of real power output of unit g, respectively.

Considering the operating status of transmission lines, the power transmitted on each line is limited as follows:

$$\begin{aligned}\left(I^t_{\mathrm{e},k} - 1\right) M &\le p^t_{\mathrm{e},k} - B_{\mathrm{e},k}\left(\gamma^{+,t}_{\mathrm{e},k} - \gamma^{-,t}_{\mathrm{e},k}\right) \\ &\le \left(1 - I^t_{\mathrm{e},k}\right) M,\ \forall t \in \mathcal{T}, k \in \mathcal{E}_{\mathrm{e}}\end{aligned} \tag{8}$$

$$-I^t_{\mathrm{e},k} P^{\max}_{\mathrm{e},k} \le p^t_{\mathrm{e},k} \le I^t_{\mathrm{e},k} P^{\max}_{\mathrm{e},k},\ \forall t \in \mathcal{T}, k \in \mathcal{E}_{\mathrm{e}} \tag{9}$$

where $\mathcal{E}_{\mathrm{e}}$ is the power transmission branch set. $B_{\mathrm{e},k}$ (S) is the reciprocal of reactance of branch k. M is a large number. $p^t_{\mathrm{e},k}$ (MW) is the active power flow on branch k. $\gamma^{+,t}_{\mathrm{e},k}$ (°) and $\gamma^{-,t}_{\mathrm{e},k}$ (°) are the bus angle at the from and to bus of branch k, respectively. $I^t_{\mathrm{e},k}$ is the operating status of branch k (1 for on-line, 0 otherwise). $P^{\max}_{\mathrm{e},k}$ (MW) is the rate of branch k.

The amount of power load shedding at each bus is constrained as follows:

$$P^t_{\mathrm{ed},i} \ge p^t_{\mathrm{elc},j} \ge 0,\ \forall t \in \mathcal{T}, j \in \mathcal{N}_{\mathrm{e}} \tag{10}$$

where $P^t_{\mathrm{ed},j}$ (MW) and $p^t_{\mathrm{elc},j}$ (MW) are the power load forecast and load shedding at bus j during t, respectively. $\mathcal{N}_{\mathrm{e}}$ is the set of power buses.

Including the power consumed by gas compressors, the real-time power balancing at each bus is depicted as follows:

$$\begin{aligned}&\sum_{g \in \mathcal{G}_j} p^t_{\mathrm{e},g} + \sum_{k \in \delta^{+}_{\mathrm{e},j}} p^t_{\mathrm{e},k} - \sum_{k \in \delta^{-}_{\mathrm{e},j}} p^t_{\mathrm{e},k} \\ &\quad = P^t_{\mathrm{ed},j} + \sum_{c \in \mathcal{E}_{\mathrm{gc},j}} p^t_{\mathrm{ge},c} - p^t_{\mathrm{elc},j},\ \forall t \in \mathcal{T}, j \in \mathcal{N}_{\mathrm{e}}\end{aligned} \tag{11}$$

where $\mathcal{G}_j$ is the set of generators at bus j. $\delta^{+}_{\mathrm{e},j}$ and $\delta^{-}_{\mathrm{e},j}$ are the set of branches to bus j and from bus j, respectively. $p^t_{\mathrm{ge},c}$ (MW) is the power consumed by gas compressor c. $\mathcal{E}_{\mathrm{gc},j}$ is the set of gas compressors fed by power bus j.

B. Gas System Model

An NG transmission system consists of sources, pipelines, compressors, etc. With consideration of the operating status, the capacity bounds of each gas source are expressed as follows:

$$Q^{\min}_{\mathrm{g},s} u^t_{\mathrm{g},s} \le q^t_{\mathrm{g},s} \le Q^{\max}_{\mathrm{g},s} u^t_{\mathrm{g},s},\ \forall t \in \mathcal{T}, s \in \mathcal{S} \tag{12}$$

where $\mathcal{S}$ is the set of gas sources. $Q^{\min}_{\mathrm{g},s}$ (MMSCF·h^{-1}) and $Q^{\max}_{\mathrm{g},s}$ (MMSCF·h^{-1}) are the minimal and maximal output of gas resource s, respectively. $u^t_{\mathrm{g},s}$ and $q^t_{\mathrm{g},s}$ (MMSCF·h^{-1}) are the on ($u^t_{\mathrm{g},s} = 1$)/off ($u^t_{\mathrm{g},s} = 0$) status and set-point of source s during time slot t, respectively.

Compared with the power flow, the gas flow changes much slower when disruptions occur. For ideal gas in horizontal isothermal pipelines, flow dynamics is controlled by partial differential equations, namely the continuity equation representing the mass conservation law and the momentum equation derived from the second Newton law. A popular way to solve partial differential equations is to discrete them over time and space into algebraic equations. Considering the operating status, the dynamic NG flow in a pipeline segment is constrained as follows:

$$\begin{aligned}&L_{\mathrm{g},k}\left(\left(v^{+,t}_{\mathrm{g},k} + v^{-,t}_{\mathrm{g},k}\right) - \left(v^{+,t\text{-}1}_{\mathrm{g},k} + v^{-,t\text{-}1}_{\mathrm{g},k}\right)\right) \\ &= 2\Delta t C_{1,k}\left(q^{-,t}_{\mathrm{g},k} - q^{+,t}_{\mathrm{g},k}\right),\ \forall t \in \mathcal{T}, k \in \mathcal{E}_{\mathrm{gp}}\end{aligned} \tag{13}$$

$$\begin{aligned}&\left(I^t_{\mathrm{gp},k} - 1\right) M \le \frac{1}{4} L_{\mathrm{g},k} C_{2,k}\left(q^{-,t}_{\mathrm{g},k} + q^{+,t}_{\mathrm{g},k}\right)\left|q^{-,t}_{\mathrm{g},k} + q^{+,t}_{\mathrm{g},k}\right| \\ &- \left(v^{+,t}_{\mathrm{g},k}\right)^2 + \left(v^{-,t}_{\mathrm{g},k}\right)^2 \le \left(1 - I^t_{\mathrm{gp},k}\right) M,\ \forall t \in \mathcal{T}, k \in \mathcal{E}_{\mathrm{gp}}\end{aligned} \tag{14}$$

$$-I^t_{\mathrm{gp},k} Q^{\max}_{\mathrm{g},k} \le q^{+,t}_{\mathrm{g},k} \le I^t_{\mathrm{gp},k} Q^{\max}_{\mathrm{g},k},\ \forall t \in \mathcal{T}, k \in \mathcal{E}_{\mathrm{gp}} \tag{15}$$

$$-I^t_{\mathrm{gp},k} Q^{\max}_{\mathrm{g},k} \le q^{-,t}_{\mathrm{g},k} \le I^t_{\mathrm{gp},k} Q^{\max}_{\mathrm{g},k},\ \forall t \in \mathcal{T}, k \in \mathcal{E}_{\mathrm{gp}} \tag{16}$$

where $\mathcal{E}_{\mathrm{gp}}$ is the set of gas pipelines. $v^{+,t}_{\mathrm{g},k}$ (psia) and $v^{-,t}_{\mathrm{g},k}$ (psia) are the pressure at from and to node of the pipeline segment, respectively. $q^{-,t}_{\mathrm{g},k}$ (MMSCF·h^{-1}) and $q^{+,t}_{\mathrm{g},k}$ (MMSCF·h^{-1})

are the volume flow rate injected to pipeline k at the from node and out of pipeline k at the to node respectively. $I^t_{\mathrm{gp},k}$ is binary variables (1 if pipeline $k$is on-line, 0 otherwise). $L_{\mathrm{g},k}$ (mile) and $Q^{\max}_{\mathrm{g},k}$ are the length and rate of pipeline segment k. $C_{1,k} = 2.7273 \times 10^4 \times 4p_{\mathrm{sc}}TZ/\pi d_k^2 T_{\mathrm{sc}}$, $C_{2,k} = 1.0138 \times 10^{14} f M_{\mathrm{g}} TZ/9\pi^{2\tilde{}} d_k^5 g_{\mathrm{c}} R$. V_{sc} and T_{sc} are the pressure and temperature of standard condition (14.65 psia, 520 R), respectively. T (R) is the average temperature of the gas in pipeline k. Z is the average gas compressibility factor. d (in) is the pipeline diameter. f is the Darcy friction factor. M_{g} is the specific natural gas molemass (17.4). g_{c} is the gravitational constant (32.1 l bm·ft·s^{-2}). R is the universal gas constant (10.73 psia·ft^3·lb^{-1}·mole^{-1}).

Compressors are installed to boost the pressure because NG suffers pressure loss in transmission due to friction. Considering the compressor operating status, the pressure ratio of each compressor is modeled as follows:

$$\begin{aligned}\left(I^t_{\mathrm{gc},c} - 1\right)\ \mathrm{M} &\le v^{+,t}_{\mathrm{g},c} - R^t_{\mathrm{g},c} v^{-,t}_{\mathrm{g},c} \\ &\le \left(1 - I^t_{\mathrm{gc},c}\right)\ \mathrm{M}\,, \forall t \in \mathcal{T}, c \in \mathcal{E}_{\mathrm{gc}} \end{aligned} \quad (17)$$

where $v^{-,t}_{\mathrm{g},c}$ (psia) and $v^{+,t}_{\mathrm{g},c}$ (psia) are the pressure of the compressor inlet and outlet node, respectively. $R^t_{\mathrm{g},c}$ is the compression ratio. $\mathcal{E}_{\mathrm{gc}}$ is the set of gas compressors. $I^t_{\mathrm{gc},c}$ is the operating status of gas compressor c (1 for on-line, 0 otherwise).

The horsepower of each compressor is calculated as follows:

$$Hp^t_{\mathrm{g},c} = \frac{a_{\mathrm{hp}} V_{\mathrm{sc}} T q^t_{\mathrm{g},c} c_{\mathrm{k}}}{T_{\mathrm{sc}} \eta_{\mathrm{g},c} (c_{\mathrm{k}} - 1)} \left(\left(R^t_{\mathrm{g},c}\right)^{\frac{c_{\mathrm{k}}-1}{c_{\mathrm{k}}}} - 1 \right), \forall t \in \mathcal{T}, c \in \mathcal{E}_{\mathrm{gc}} \quad (18)$$

$$0 \le Hp^t_{\mathrm{g},c} \le I^t_{\mathrm{gc},c} HP^{\max}_{\mathrm{g},c},\ \forall t \in \mathcal{T}, c \in \mathcal{E}_{\mathrm{gc}} \quad (19)$$

where $Hp^t_{\mathrm{g},c}$ (hp) is the horsepower of gas compressor c during time slot t. $HP^{\max}_{\mathrm{g},c}$ (hp) is the maximum horsepower of compressor c. $q^t_{\mathrm{g},c}$ (MMSCF·h^{-1}) is the volume flow rate from the compressor inlet to the outlet. a_{hp} is constant. c_{k} is the gas specific heat ratio. $\eta_{\mathrm{g},c}$ is the compressor efficiency.

At each gas node, the pressure is constrained as follows:

$$V^{\min}_{\mathrm{g},j} \le v^t_{\mathrm{g},j} \le V^{\max}_{\mathrm{g},j},\ \forall t \in \mathcal{T},\ j \in \mathcal{N}_{\mathrm{g}} \quad (20)$$

where $\mathcal{N}_{\mathrm{g}}$ is the set of gas nodes. $V^{\min}_{\mathrm{g},j}$ (psia) and $V^{\max}_{\mathrm{g},j}$ (psia) are minimal and maximal allowed pressure at node j, respectively. $v^t_{\mathrm{g},j}$ (psia) is the pressure at node j during time slot t.

Load shedding at each node is constrained as follows:

$$Q^t_{\mathrm{gd},j} \ge q^t_{\mathrm{glc},j} \ge 0,\ \forall t \in \mathcal{T},\ j \in \mathcal{N}_{\mathrm{g}} \quad (21)$$

where $Q^t_{\mathrm{gd},j}$ (MMSCF·h^{-1}) and $q^t_{\mathrm{glc},j}$ (MMSCF·h^{-1}) are the NG load forecast and NG load shedding at node j during time slot t, respectively.

Including the NG consumed by GFGs, the node gas balance equation is described as follows:

$$\begin{aligned}&\sum_{s \in \mathcal{S}_j} q^t_{\mathrm{g},s} + \sum_{k \in \delta^+_{\mathrm{g},j}} q^{+,t}_{\mathrm{g},k} - \sum_{k \in \delta^-_{\mathrm{g},j}} q^{-,t}_{\mathrm{g},k} + \sum_{c \in \mathcal{C}^+_{\mathrm{g},j}} q^t_{\mathrm{g},c} - \sum_{c \in \mathcal{C}^-_{\mathrm{g},j}} q^t_{\mathrm{g},c} \\ &\quad = Q^t_{\mathrm{gd},j} + \sum_{g \in \mathcal{G}_{\mathrm{eg},j}} q^t_{\mathrm{eg},g} - q^t_{\mathrm{glc},j},\ \forall t \in \mathcal{T}, j \in \mathcal{N}_{\mathrm{g}} \end{aligned} \quad (22)$$

where $\mathcal{S}_j$ is the set of gas sources at node j. $\delta^+_{\mathrm{g},j}$ and $\delta^-_{\mathrm{g},j}$ are the set of gas pipelines to node j and from node j, respectively. $\mathcal{C}^+_{\mathrm{g},j}$ and $\mathcal{C}^-_{\mathrm{g},j}$ are the set of gas compressors to and from node j, respectively. $\mathcal{G}_{\mathrm{eg},j}$ is the set of GFGs fed by node j. $q^t_{\mathrm{eg},g}$ (MMSCF·h^{-1}) is the gas required by gas-fired generator g.

C. Interdependence Model

The dependence among the power system and the NG system is bi-directional. GFGs converter energy stored in NG into electrical energy and participate in the NG system as loads. The NG consumed by each gas-fired generator is determined by its output and efficiency as follows:

$$q^t_{\mathrm{eg},g} = C_{\mathrm{g2e},g} \eta_{\mathrm{g2e},g} p^t_{\mathrm{e},g}, \forall t \in \mathcal{T},\ g \in \mathcal{G}_{\mathrm{eg}} \quad (23)$$

where $\mathcal{G}_{\mathrm{eg}}$ is the set of GFGs. $C_{\mathrm{g2e},g}$ is constant. $\eta_{\mathrm{g2e},g}$ is the energy conversion efficiency of generator g.

Similarly, gas compressors driven by electricity act as power consumers in the power system. The power required by each compressor is determined by its horsepower as follows:

$$p^t_{\mathrm{ge},c} = \eta_{\mathrm{e2g},c} Hp^t_{\mathrm{g},c},\ \forall t \in \mathcal{T}, c \in \mathcal{E}_{\mathrm{gc}} \quad (24)$$

where $\mathcal{E}_{\mathrm{gc}}$ is the set of gas compressors driven by electricity. $\eta_{\mathrm{e2g},c}$ is a constant.

IV. Resilience Assessment Method and Indices

This section introduces the resilience assessment method and indices based on the integration of the models built in Section II and Section III.

A. Assessment Method

The assessment procedure shown in Fig. 2 is described in details as follows:

Step 1: Data acquisition.

Step 1.1: System data, including the system topology of the power and NG system; power and NG load forecast; system operation constraints, such as the bounds of power generators, transmission lines, gas sources, NG pipelines and so on; structure features and values of exposed components, such as design wind and rainfall, component value, replace cost of components and so on; etc.

Step 1.2: Geographic data, including locations and local terrain features of exposed components. This data are used to calculate the wind and rainfall intensity at component sites as introduced in [27].

Step 1.3: Hurricane event data, such as the tme-varying hurricane center location, translation speed, moving direction, central pressure deficiency and coefficients needed in the hurricane wind field model as described in [27]. The event information is gained from forecast information, simulation results, or historical records depending on the application purpose.

Step 2: Component failure probability calculation. At each time slot, update the hurricane center location,

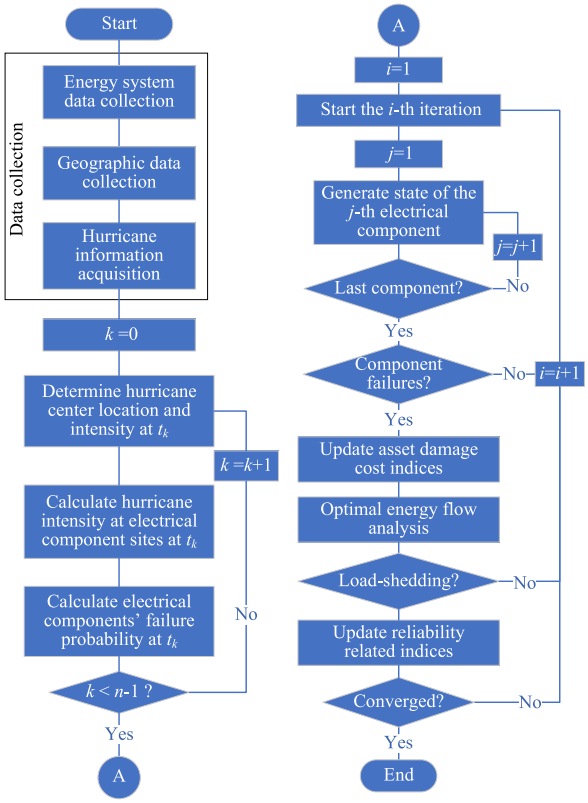

Fig. 2. Flowchart of interdependent energy network resilience assessment under hurricanes.

calculate the hurricane intensity at the location of exposed components using the wind field model introduced in [27], then input the results to the models built in Section II determine component failure probabilities.

Step 3: System state generation by Monte Carlo simulation. It is assumed no component fails at the beginning of a new iteration. Then from time slot $t = 1$, take an exposed component (tower or conductor segment), if it has been simulated to be down, proceed to the next exposed component; else, simulate the component operating state by Monte Carlo simulation. A random number R_i distributed uniformly in $[0, 1]$ is generated first, then it is compared with the component failure probability at time slot t. If the component failure probability is smaller than R_i, the component is simulated to be up during t, record the simulation result and proceed to time slot $t + 1$. Otherwise, record the component state as failed t, and it would keep failed during the left time. Continue the simulation until the states in $\mathcal{T}$ of all exposed components are generated. In this paper, it is assumed that failures of towers and conductor segments are independent. The failure probability and state of a transmission line can be determined according to the series theory with given failure probability and state of towers and conductor segments in this line. The power system state is determined by combination of transmission lines' states.

Step 4: Resilience indices calculation. In $\mathcal{T}$, with a system state generated in Step 3), check if there any failed components. If no, turn to Step 3 to start the next iteration. If yes, calculate and update infrastructure indices. Then, conduct the integrated energy flow to determine if the power and gas loads can be satisfied in $\mathcal{T}$. If yes, turn to Step 3. If no, record the optimal power and gas load curtailments in every time interval of $\mathcal{T}$. Update operational indices and check if converged. If no, start the next iteration. If yes, end the simulation.

In Step 4, the integrated energy flow is formulated as an optimization problem with the objective of minimum joint load shedding as follows:

$$\min_{\mathbf{y}\in\mathbf{Y}} \mathbf{d}^{\mathrm{T}}\mathbf{y} = \sum_{t\in\mathcal{T}} \left\{ \underbrace{\sum_{j\in\mathcal{N}_{\mathrm{e}}} p^{t}_{\mathrm{elc},j}}_{\text{Power Load Shedding}} + \underbrace{\sum_{j\in\mathcal{N}_{\mathrm{g}}} w_{\mathrm{g},j} q^{t}_{\mathrm{glc},j}}_{\text{Gas Load Shedding}} \right\} \tag{25}$$

where $w_{\mathrm{g},j}$ is the weight factor of the gas load at node j. $\mathbf{y} = \{p^t_{\mathrm{e},g}, p^t_{\mathrm{e},k}, \gamma\mathrm{e}, k^{+,t}, \gamma\mathrm{e}, k^{-,t}, q^t_{\mathrm{g},s}, p^{+,t}_{\mathrm{g},k}, p^{-,t}_{\mathrm{g},k}, q^{+,t}_{\mathrm{g},k}, q^{-,t}_{\mathrm{g},k}, p^{+,t}_{\mathrm{g},c}, p^{-,t}_{\mathrm{g},c}, Hp^t_{\mathrm{g},c}, g^t_{\mathrm{eg},g}, p^t_{\mathrm{ge},c}, p^t_{\mathrm{elc},j}, q^t_{\mathrm{glc},j}, I^t_{\mathrm{gc},c}, I^t_{\mathrm{gp},k}, u^t_{\mathrm{g},s}\}$ is the decision variables. Y is the constraint set for real-time operation of the interdependent energy system as described in (8)–(24).

Problem (25) is a non-convex mixed-integer optimization problem, due to the non-convexity of (14). The piece-wise linear method [28] is adopted to approximate (14) into a set of linear constraints with auxiliary variables, formulating a mixed-integer linear programming counterpart of (25), which can be solved efficiently by off-shore solvers, e.g., Gurobi [29] in this paper.

B. Assessment Indices

Operational indices related to load shedding are used to reflect the ability of interdependent power and NG systems to provide adequate service to customers under hurricanes. Besides, infrastructure indices are employed to describe network physical damages. Overall indices are proposed to quantify the total cost of load interruption and component damage.

1) Operational Indices: At load point level, in addition to power demand not supplied and related cost at buses, gas demand not supplied and related cost at gas nodes are used as time-varying indices to reveal how the hurricane affects the interdependent energy system temporally and spatially, as follows:

$$DNS^t_{\mathrm{e},j} = \sum_{i\in S^t_{\mathrm{e}}} \pi^{i,t}_{\mathrm{elc}} \cdot DNS^{i,t}_{\mathrm{e},j} \tag{26}$$

$$C^t_{\mathrm{elc},j} = \Delta t \cdot DNS^t_{\mathrm{e},j} \cdot C^t_{\mathrm{e},j} \tag{27}$$

where $DNS^t_{\mathrm{e},j}$ (MW) is the expected power demand not supplied at bus j during time slot t. S^t_{e} is the set of power system states with power load curtailment during time slot t. $\pi^{i,t}_{\mathrm{elc}}$ is the associated probability of power system state i. $DNS^{i,t}_{\mathrm{e},j}$ (MW) is the power demand not supplied at the bus j associated with

system state i during time slot t. It is equal to $p^t_{\text{elc},i}$ in (25) associated with system state i. $C^t_{\text{elc},j}$ and $C^t_{\text{e},j}$ (M$) are the cost of power load shedding and the per-unit interruption cost at bus j, respectively.

$$DNS^t_{\text{g},j} = \sum_{i \in S^t_{\text{g}}} \pi^{i,t}_{\text{glc}} \cdot DNS^{i,t}_{\text{g},j} \tag{28}$$

$$C^t_{\text{glc},j} = \Delta t \cdot DNS^t_{\text{g},j} \cdot C^t_{\text{g},j} \tag{29}$$

where $DNS^t_{\text{g},j}$ (MMSCF·h^{-1}) is the expected NG demand not supplied at node j during time slot t. S^t_{g} is the set of power system states with gas load curtailment during time slot t. $\pi^{i,t}_{\text{glc}}$ is the associated probability of power system state i. $DNS^{i,t}_{\text{g},j}$ (MMSCF·h^{-1}) is the gas demand not supplied at node j associated with system state i. It is equal to $q^t_{\text{glc},j}$ in (25) associated with system state i. $C^t_{\text{glc},j}$ and $C^t_{\text{g},j}$(M$) are the cost of gas load shedding and per-unit interruption cost at node j, respectively.

At the system level, hourly-varying power and gas demand not supplied are calculated as follows:

$$DNS^t_{\text{e}} = \sum_{j=1}^{n_{\text{el}}} DNS^t_{\text{e},j} \tag{30}$$

$$DNS^t_{\text{g}} = \sum_{j=1}^{n_{\text{gl}}} DNS^t_{\text{g},j} \tag{31}$$

where DNS^t_{e} (MW) is the power system demand not supplied during time slot t. DNS^t_{g} (MMSCF·h^{-1}) is the gas system demand not supplied during time slot t. n_{el} and n_{gl} are the number of power buses and gas nodes with load, respectively.

2) Infrastructure Indices: Operational indices can reflect the hurricane's impact on the ability of satisfying demands. However, as the power system is designed according to some reliability criteria, such as N-k, in some situations, the hurricane destroys some components but may result in no load curtailment. The impact of hurricanes cannot be reflected only by operational indices and the time-varying infrastructure physical damage should also be accounted. Therefore, the asset damage cost is proposed as follows:

$$C^t_{\text{ad}} = \sum_{i \in S^t_{\text{ad}}} \left(\pi^{i,t}_{\text{ad}} \cdot \sum_{j=1}^{n_{\text{ad}}} C^{j,t}_{\text{cm}} \right) \tag{32}$$

where C^t_{ad} (M$) is asset damage cost during t. S^t_{ad} is the set of system states with components that are damaged during t. $\pi^{i,t}_{\text{ad}}$ is the associated probability of system state i. n_{ad} is the number of components that are damaged during t associated with system state i. $C^{j,t}_{\text{cm}}$ (M$) is the repair or replacement cost of damaged component j.

3) Overall Indices: Total power energy not supplied, $TENS_{\text{e}}$ (MWh), total gas energy not supplied, $TENS_{\text{g}}$ (BTU), as well as total cost $TCOST$ (M$) of the interdependent power and NG systems, are developed as follows, to provide a holistic view of the hurricane impact on each individual system and the interdependent energy system:

$$TENS_{\text{e}} = \sum_{t=1}^{\text{T}} \Delta t \cdot DNS^t_{\text{e}} \tag{33}$$

$$TENS_{\text{g}} = \sum_{t=1}^{\text{T}} \Delta t \cdot DNS^t_{\text{g}} \tag{34}$$

$$TCOST = \sum_{t=1}^{\text{T}} \left(C^t_{\text{ad}} + \sum_{i=1}^{n_{\text{el}}} C^t_{\text{elc},i} + \sum_{j=1}^{n_{\text{gl}}} C^t_{\text{glc},j} \right) \tag{35}$$

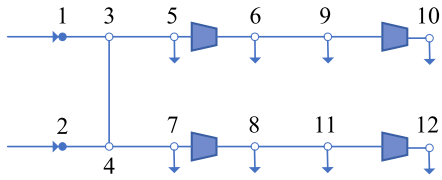

Fig. 3. The 12-node NG transmission system.

TABLE I
NODES IN THE GAS SYSTEM

Node	$q^{\max}_{\text{g},s}$ (MMSCF·h^{-1})	$q^{\min}_{\text{g},s}$ (MMSCF·h^{-1})	$d_{\text{g},j}$ (MMSCF·h^{-1})	$p^{\max}_{\text{g},j}$ (psia)	$p^{\min}_{\text{g},j}$ (psia)
1	50	0	0	1200	600
2	50	0	0	1200	600
3	0	0	1.438	1200	500
4	0	0	0.818	1200	500
5	0	0	1.3248	1200	400
6	0	0	1.0424	1200	400
7	0	0	1.3450	1200	400
8	0	0	1.1363	1200	400
9	0	0	2.7253	1200	400
10	0	0	2.0787	1200	400
11	0	0	1.0424	1200	400
12	0	0	4.4385	1200	400

TABLE II
PIPELINES IN THE GAS SYSTEM

Pipeline	From node	To node	$C_{1,k}$	$C_{2,k}$	$q^{\max}_{\text{g},k}$ (MMSCF·h^{-1})
1	1	3	1196.6885	88.56261	12.9196
2	2	4	1196.6885	88.56261	12.9357
3	3	4	1196.6885	88.56261	15.5040
4	3	5	1189.3805	87.12770	15.5062
5	4	7	1189.3805	87.12770	14.7093
6	6	9	1189.3805	87.12770	12.5349
7	8	11	1643.6379	206.4352	8.8203

V. CASE STUDIES

Under a simulated hurricane, the IEEE 24-reliability test system and the 12-node NG transmission system are used to validate the effectiveness of the proposed method.

A. Test Systems

1) 12-node NG Transmission System: The 12-node NG test system shown in Fig. 3 is modified from the 15-node NG transmission system in [30]. It has 12 nodes, 7 pipelines and 4 compressors as described in Table I, Table II and Table III, respectively. The daily gas load profile is referred to [31].

TABLE III
COMPRESSORS IN THE GAS SYSTEM

Compressor	From node	To node	Fed by power bus	$R_{g,c}$	$HP_{g,c}^{max}$
1	5	6	8	1.37	6206.7185
2	7	8	19	1.378	5928.89065
3	9	10	20	1.37	5017.3863
4	11	12	14	1.378	3555.2062

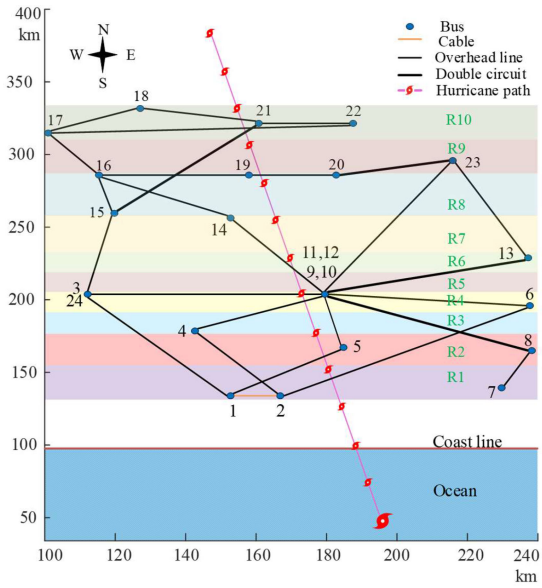

Fig. 4. IEEE 24-reliability test system under the hurricane.

2) IEEE 24-Reliability Test System: The IEEE 24-reliability test system is projected to a 150*200 km open country area approximately located from 30.52° N to 32.32° N and 87.68° W to 89.25° W). The simulated hurricane with detailed information in [27] is used in this paper. The hurricane center locations are marked by red symbols along the path it moves from the south to the north in flat Earth coordinates with the origin (29.42° N, 89.24° W) is shown in Fig. 4.

The design wind speed (50-year return period) of region R1 is assumed to be 50 m· s^{-1} according to ASCE 7 windspeed map. The design wind speed decreases by 1 for each region from the south to the north. All the components of the test system are assumed to have the same design rainfall rate which is set to 30 mm· h^{-1}. The segment length in (3) of transmission line conductors is taken as a typical span length of 350 m. The latitude and longitude location of electrical components are extracted according to the figure in [32]. $a_{cs,k}$, $b_{cs,k}$, and $c_{cs,k}$ in (3) are set to 10.5497, 3.0385, −31.0087, respectively. The value and replacement cost of a tower is set to 0.25 M$ and 0.45 M$, respectively. The value and replacement cost of conductors is set to 0.052 M$ · km^{-1} and 0.072 M$ · km^{-1}, respectively. All power loads are assumed to be composite customers with $C_{e,j}^{t}$ in (27) as 29.41 $ · kW^{-1} [8].

Three subcases are used to validate the proposed method as follows:

TABLE IV
GFGS IN THE POWER SYSTEM IN CASE I-B)

GFP	Power Bus	Capacity (MW)	Fed by Gas Node	η_{g2e}
1	7	100	8	0.5
2	7	100	8	0.5
3	7	100	8	0.5
3	13	197	6	0.5
4	13	197	6	0.5
5	13	197	6	0.5
6	15	12	10	0.5
7	15	12	10	0.5
8	15	12	10	0.5
9	15	12	10	0.5
10	15	12	10	0.5
11	15	155	10	0.5
12	21	400	10	0.5
13	22	50	8	0.5
14	22	50	8	0.5
15	22	50	8	0.5
16	22	50	8	0.5
17	22	50	8	0.5
18	22	50	8	0.5

TABLE V
COMPARISON OF 3 SUBCASES

	Results	case I-a)	case I-b)	case I-c)
Objective values (M$)	Asset damage cost	5.8616	5.8616	5.9074
	Power load curtailment cost	3.0691	7.8026	6.8396
	Gas load curtailment cost	0	0.0342	0.0360
	Total cost	8.9307	13.6984	12.7829
Energy not supplied	Power (MWh)	104.3545	265.3054	232.5601
	Gas (Btu)	0	1.1794×10^9	1.2412×10^9
	Total (MWh)	104.3545	610.95334	596.3241

Case I-a: Independent power system and NG system under the simulated hurricane. There are no power generators fueled by gas. Besides, all gas compressors are driven by gas turbines.

Case I-b: Interdependent power and NG systems under the simulated hurricane. All gas compressors are driven by electricity as described in Table III. Besides, the 11 generators at power bus 7, 13, 15, 21 and 22 are assumed to be GFGs and fed by gas node 8, 6, 10, 10 and 8, respectively, as listed in Table IV.

Case I-c: Reduced capacity of GFGs. Compared to case I-b), all generators with a total capacity of 215 MW at power bus 15 are no longer fueled by NG. The total capacity of GFGs is reduced from 1806 MW in case I-b) to 1591 MW in this case.

Besides, the total power load is enlarged by 1.4 times for all the three subcases. The power system load profile is extracted from [32] according to the hurricane date, time and duration.

B. Simulation Results

The overall comparison of the three subcases is shown in Table V. Under the simulated hurricane, the independent power system in case I-a suffers $TENS_e$ as 104.3545 MWh and $TCOST$ as 8.9307M$. In comparison with case I-a), the interdependent power and NG systems in case I-b) suffer $TENS_e$ as 265.3054 MWh, increasing sharply by 154.2347%, $TENS_g$ from 0 to 1.1794×10^9 BTU and $TCOST$ as 13.6984M$. The results indicate that the interdependence amplifies the hurricane impact by introducing the disruptions originally occurring in the power

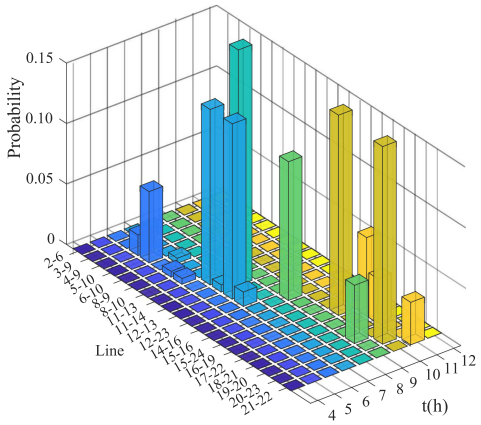

Fig. 5. Failure probability of power transmission lines under the hurricane [27].

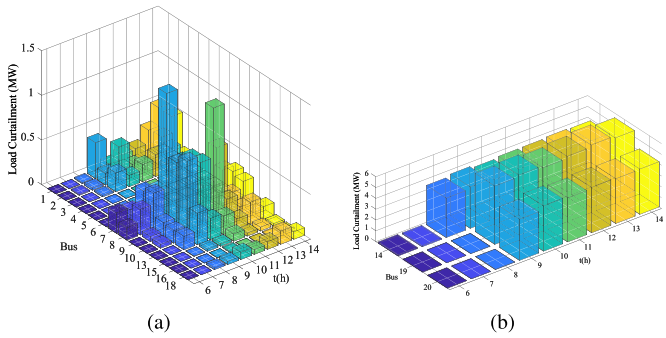

Fig. 6. Load curtailments at power buses in case I-a).

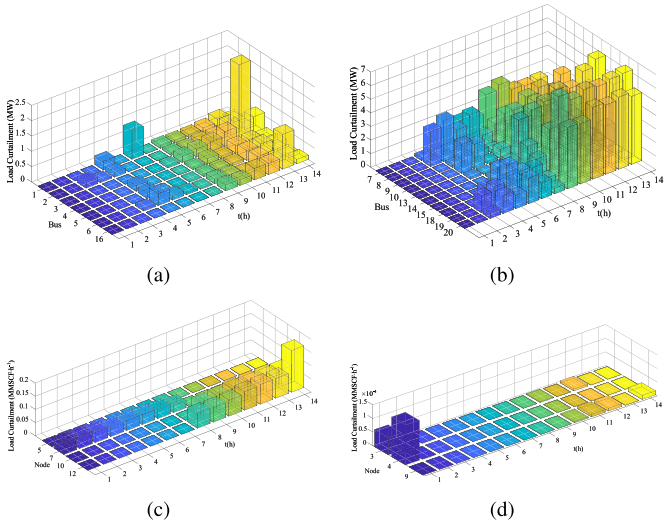

Fig. 7. Load curtailments at power buses and gas nodes in case I-b).

system to the connected NG system and further increasing the amount of power load shedding. When the capacity of GFGs is reduced in case I-c), there is an apparent decline in the power load shedding while the gas load shedding increases slightly in comparison with that in case I-b).

Besides, the expected number of damaged power components and the cost to repair or replace these components are with slight difference in the three subcases due to the effect of simulation process.

1) Impact of the Hurricane: The variation of transmission line failure probabilities over time during the hurricane event is depicted in Fig. 5. Due to the far distance from the hurricane, line 7–8 (from bus 7 to bus 8), 13–23 and 16–17 are almost unaffected by the hurricane. Line 1–3, 1–5, 2–4 and 2–6 also display lower failure probabilities than the left lines because firstly the component design criteria of R1 is higher than other the regions, and secondly the wind attack angles are not such adverse. The large wind attack angle also results in lower failure probability of line 15–21 in comparison with lines in Fig. 5, although it crosses the maximum wind radius of the hurricane during time lot 7 to 9. Line 11–14 is with the highest failure probability among all line during time lot 7, followed by line 16–19 with the second highest one during time lot 9 and line 20–23 with the third highest one also during time lot 9. Line 11–14, 16–19 and 20–23 show the top 3 failure probabilities because they cross the hurricane maximum wind radius and are attacked with unfavorable wind attack angles.

From a space perspective, lines in R1 and R2 are generally with lower failure probabilities than lines in other regions primarily because of the component wind design value decreases from R1 to R10 gradually. Lines in R5 to R8 such as 11–13, 12–13, 11–14, 14–16, 16–19, 20–23 are not as resistant as other regions to the simulated hurricane.

The variation of bus load curtailments over $\mathcal{T}$ are shown in Fig. 6. Load shedding occurs at bus 1 to 5, 8 to 10, 14 to 16, and 18 to 20, while loads on the left buses are rarely affected by the hurricane. Bus 19,14 and 20 have the top 3 highest load curtailment which is consistent with the results shown in Fig. 5. Line 11–14, 14–16, 16–19, 19–20, and 20–23 are with a greater likelihood to be damaged by the hurricane, which leads to the relatively high load curtailment at bus 14, 19, and 20.

2) Combined Impact of Hurricane and Interdependence: The time-varying load curtailment at power buses and gas nodes is given in Fig. 7. It can be seen from Fig. 7(a) and Fig. 7(b) that load shedding is inevitable at all power buses with load.[2] Load curtailment at bus 14, 19 and 20 are significantly higher than others as in case I-a). In comparison with case I-a), all power load buses experience more load shedding in case I-b) due to the insufficient power generation caused by the shortage of gas fuel. By comparing Fig. 6(a) and Fig. 7(a), it can be seen load shedding at bus 7 to 10, 13 to 16, and 18 to 20 increases sharply.

Besides, power load shedding in case I-a) starts from $t = 5$, while in case I-b), both the power system and the NG system experience load shedding over the whole $\mathcal{T}$ due to the negative impact of interdependence. The difference demonstrates the different characteristics of electricity and NG. NG can be stored in pipelines for later use to achieve optimal objectives.

[2]In IEEE-24 Reliability Test System, there are 17 power buses with load out of 24 buses.

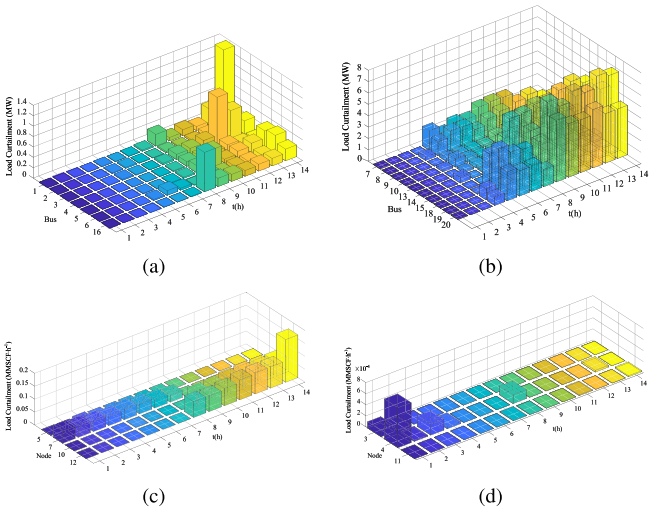

Fig. 8. Load curtailments at power buses and gas nodes in case I-c).

Node 12, 10 and 7 have the top three high load shedding. NG supplied to 12 has to be through compressor 11–12 which gains electricity from power bus 14. However, bus 14 is easy to be isolated with failures of power line 11–14 and 14–16. Unfortunately, the isolation of bus 14 interrupts power supplied to compressor 11–12, forces the compressor out and results in load shedding at node 12. Node 10 is the fuel source for 7 GFGs with a total capacity of 615 MW. Although 5 GFGs with a capacity of 12MW at bus 15 are committed to be down according to the UC result, node 12 still affords fuel for 555 MW power generation capacity, which puts much stress on node 12 and challenges its ability to satisfy all loads connected to it. Node 7 suffers the third high load shedding because it is set to have much lower weight factor than other nodes except node 5 which has the same weight factor as node 7.

Take an example to explain how the interdependence amplifies the adverse hurricane impact. For a power system state with transmission line 4–9 failed from time slot 5, 16–19 and 20–23 failed from time slot 9, 18–21 failed from time slot 10, bus 19 and 20 are isolated from time slot 9. Loads at power bus 19 and 20 are totally shed from time slot 9 due to bus isolation. As a result, gas compressor 7–8 (from node 7 to node 8) and 9–10 are forced out immediately, indicating that interruptions in the power system have spread to the NG system. When compressor 9–10 is out of service from time slot 9, all load at gas node 10 has to be shed immediately, which leads to cut off of gas fuel supplied to GFGs at power bus 15 and 21 and they are forced out from time slot 9. The impact of load shedding in the NG system loops back to the power system. From time slot 9, the NG stored at pipeline 8–11 is extracted to satisfy loads at node 8, 11 and 12. In order to store as much as NG in the pipeline 8–11, the NG system is optimized to increase the gas pressure at node 8, 11 and 12 from time slot 1 to 9. However, the gas stored is limited and due to the lower bound of node pressure constraint, the load at node 12 cannot be fully satisfied from time slot 13. Besides, in order to satisfy gas loads with higher priority, gas node 8 cannot provide gas to GFGs as much as required. As a result, GFGs fed by gas node 8 are with low output even out of service most of the time. Power generation shortage results in power load shedding at bus 13, 16, and 18.

3) Impact of the Interdependence: In comparison with case I-b), the total capacity of the GFGs is reduced by 215 MW, all 6 generators at power bus 15 are no longer fueled by NG in case I-c). As a result, as shown in Table V, $TENS_{\mathrm{e}}$ decreases by 12.3425% from 265.3054 MWh in case I-b) to 232.5601 MWh, while $TENS_{\mathrm{g}}$ increases slightly by 5.2400% from 1.1794×10^9 Btu in case I-b) to 1.2412×10^9 Btu. $TCOST$ is reduced by 6.6833% from 13.6984M$ in case I-b) to 12.7829M$ due to different factors of gas loads. Detailed time-varying load shedding at power buses and gas nodes is given in Fig. 8. It is obvious the higher the interdependence is, the higher risk it may introduce. To prepare the connected system more effectively, more attention should be paid to the crucial interfaces.

C. Suggestions

According to the simulation results, suggestions can be provided to the system operators to allow directed actions to be planned and carried out before the advent of hurricanes. From the short-term perspective, for the simulated hurricane, deployment of the energy storage and the portable power generation at buses with load shedding, e.g., 14, 19 and 20, can help to reduce the risk of load curtailment and promote system resilience. Besides, the interlinks should be paid with special attention. For example, place backup generators at the location of electricity-driven gas compressors and use gas storage facilities at power plants to store gas for emergency use. For example, in case I-b) if compressor 7–8 and 11–12 are equipped with backup generators, the $TENS_{\mathrm{e}}$ would decrease significantly by 47.8130% from 265.3054 MWh to 138.4549 MWh, while $TENS_{\mathrm{g}}$ would decrease dramatically by 72.0653% from 1.1794×10^9 Btu to 3.3449×10^8 Btu. Line pack storage could be considered as a helpful tool for enhancing the system preparedness in emergency conditions. The adjustment of unit commitment status is also a potential strategy. Some generators will be committed to minimize the load shedding cost. From a long-term view, the upgrade of weak transmission lines with much strict design criteria and optimization of generation capacity and relocation can help to build a more resilient energy system.

VI. Conclusion

In this paper, a jointed data and model approach for resilience assessment is proposed integrating component failure models under hurricanes and interdependent energy system models to quantify the hurricane impacts on the performance of interdependent power and NG systems. The simulation results reveal that the failure probabilities of transmission lines varies from line to line and time to time for the same line. The time-space varying transmission line failure probabilities can help to identify the weak parts of power systems under the impacts of the simulated hurricane. Besides, it can also be concluded from the simulation results that the interdependence could amplify the adverse impacts of hurricanes on the power system and transfer

the impacts to the NG system. It verified in the case studies that if the interdependence between the energy systems is reduced, for example by reducing the capacity ratio of GFGs or by equipping compressors with backup generators, the total cost caused by the event can be reduced. Based on the simulation results, proactive strategies, e.g., the allocation of external energy sources can be taken to mitigate the hurricane impact and reduce hazard cost.

In the future, resilience metrics, restoration strategy optimization and resilience improvement strategies considering the long-term impacts of hurricanes can also be developed based on the extension of this work.

APPENDIX
TWO-STAGE ROBUST UNIT COMMITMENT MODEL FOR INTEGRATED ENERGY SYSTEMS

Considering the uncertain transmission lines failures under hurricanes, we have proposed a two-stage robust unit commitment (UC) model for the independent energy systems. First, this UC is conducted to generate the commitment status and reserve of generators; then the results are input to the resilience assessment in Section IV.

A. Objective Function

The objective is to minimize the start-up, shutdown, fuel and reserve cost of generators, together with the worst case load shedding cost considering the failures and operation status of transmission lines, as follows:

$$\min_{\mathbf{x}\in\mathbf{X}} f(\mathbf{x}) + \max_{\boldsymbol{\xi}\in\mathcal{U}}[\mathcal{Q}(\mathbf{x},\boldsymbol{\xi})] \tag{A1}$$

$$f(\mathbf{x}) = \mathbf{c}^{\mathrm{T}}\mathbf{x} = \sum_{t\in\mathcal{T}}\sum_{g\in\mathcal{G}}\{c_{\text{start},g}\alpha_g^t + c_{\text{shut},g}\beta_g^t + b_g u_g^t + \left[a_g P_{e,g}^t + c_{\text{r},g}R_{e,g}^t\right]\Delta t\} \tag{A2}$$

$$\mathcal{Q}(\mathbf{x},\boldsymbol{\xi}) = \min_{\mathbf{y}\in\mathbf{Y}} \mathbf{d}^{\mathrm{T}}\mathbf{y} = VOLL\sum_{t\in\mathcal{T}}\sum_{j\in\mathcal{N}_{\text{e}}} p_{\text{elc},j}^t\Delta t$$
$$\text{s.t.}\quad \mathbf{E}\mathbf{y} \geq \mathbf{h} - \mathbf{G}\mathbf{x} - \mathbf{M}\boldsymbol{\xi} \tag{A3}$$

where $\boldsymbol{\xi}$ is the uncertainty variable vector. $c_{\text{start},g}$ ($), $c_{\text{shut},g}$ ($), and $c_{\text{r},g}$ ($/MWh^{-1}) are the start-up, shutdown, and reserve cost of generator g, respectively. a_g, b_g ($\cdot$ MWh^{-1}) are fuel cost of generator g. $\mathbf{x} = \{\alpha_{\text{e},g}^t, \beta_{\text{e},g}^t, u_{\text{e},g}^t, P_{\text{e},g}^t, R_{\text{e},g}^t, P_{\text{e},k}^t, \theta_{\text{e},k}^{+,t}, \theta_{\text{e},k}^{-,t}, Q_{\text{g},s}^t, V_{\text{g},k}^{+,t}, V_{\text{g},k}^{-,t}, Q_{\text{g},k}^{+,t}, Q_{\text{g},k}^{-,t}, V_{\text{g},c}^{+,t}, V_{\text{g},c}^{-,t}, HP_{\text{g},c}^t, Q_{\text{eg},g}^t, P_{\text{ge},c}^t\}$ is the first stage decision variables. $\alpha_{\text{e},g}^t$ and $\beta_{\text{e},g}^t$ are the start-up and shut-down command of generator g, respectively. $u_{\text{e},g}^t$ is binary variables, 1 if generator g is on-line, 0 otherwise. $P_{\text{e},g}^t$ (MW) is the output of generator g. $R_{\text{e},g}^t$ (MW) is the reserve capacity of generator g. $P_{\text{e},k}^t$ is the power transfer on line k. $\theta_{\text{e},k}^{+,t}, \theta_{\text{e},k}^{-,t}$ are the angle at from and to bus of line k, respectively. $Q_{\text{g},s}^t$ (MMSCF$\cdot$ h^{-1}) is the gas supply of source s. $V_{\text{g},k}^{+,t}, V_{\text{g},k}^{-,t}$ (psia) are the pressure at from and to node of pipeline k, respectively. $Q_{\text{g},k}^{+,t}$ (MMSCF$\cdot$h^{-1}), $Q_{\text{g},k}^{-,t}$ are gas injection to and extraction from pipeline k, respectively. $V_{\text{g},c}^{+,t}, V_{\text{g},c}^{-,t}$ (psia) are pressure at outlet and inlet node of compressor c, respectively. $HP_{\text{g},c}^t$ (hp) is the horsepower of compressor c. $Q_{\text{eg},g}^t$ (MMSCF$\cdot$h^{-1}) is the gas consumption of generator g. $P_{\text{ge},c}^t$ (MW) is the electricity consumption of compressor c. *VOLL* ($\cdot$MWh^{-1}) is the value of load loss. $\mathbf{y} = \{p_g^t, p_{\text{e},k}^t, \gamma_{\text{e},k}^{+,t}, \gamma_{\text{e},k}^{-,t}, p_{\text{elc},j}^t\}$ is the second stage decision variables. $p_{\text{e},g}^t$(MW) is the active power output of generator g. $p_{\text{e},k}^t$ (MW) is the power transfer on line k. $\gamma_{e,k}^{+,t}, \gamma_{e,k}^{-,t}$ are the angle at from and to bus of line k, respectively. $p_{\text{elc},j}^t$ (MW) is the power load shedding at bus j. $\mathbf{X}$ is the constraint set for the day-ahead scheduling, including both electrical systems and gas systems, depicted in Part B. $\mathbf{Y}$ is the constraint set for real-time operation of electrical systems after the realization of transmission lines, depicted in Part C. The constraint set for uncertainty variables, i.e., $\mathcal{U}$ is illustrated in Part D.

B. First-Stage Constraint Set

The first-stage constraint set, i.e., $\mathbf{X}$, includes the constraints for 1) power system and 2) gas system.

1) Power System: The technical constraints of generators, transmission lines, power balance and reserve requirements are formulated as follows:

$$\alpha_{\text{e},g}^t - \beta_{\text{e},g}^t = u_{\text{e},g}^t - u_{\text{e},g}^{t-1}, \forall t\in\mathcal{T}, g\in\mathcal{G} \tag{A4}$$

$$\sum_{q=t-\text{UT}_g+1}^{t} \alpha_{\text{e},g}^q \leq u_{\text{e},g}^t, \forall t\in\{\text{UT}_g,\ldots,T\}, g\in\mathcal{G} \tag{A5}$$

$$\sum_{q=t-\text{DT}_g+1}^{t} \beta_{\text{e},g}^q \leq 1 - u_{\text{e},g}^t, \forall t\in\{\text{DT}_g,\ldots,T\}, g\in\mathcal{G} \tag{A6}$$

$$u_{\text{e},g}^t = u_{\text{e},g}^0, \forall t\in\{\Delta t,\ldots,\text{UT}_{\text{r}}+\text{DT}_{\text{r}}\}, g\in\mathcal{G} \tag{A7}$$

$$u_{\text{e},g}^t P_{\text{e},g}^{\min} \leq P_{\text{e},g}^t - R_{\text{e},g}^t, \forall t\in\mathcal{T}, g\in\mathcal{G} \tag{A8}$$

$$P_{\text{e},g}^t + R_{\text{e},g}^t \leq P_{\text{e},g}^{\max} u_{\text{e},g}^t\Delta t, \forall t\in\mathcal{T}, g\in\mathcal{G} \tag{A9}$$

$$0 \leq R_{\text{e},g}^t \leq \text{R}_{\text{e},g}^{10+} u_{\text{e},g}^t, \forall t\in\mathcal{T}, g\in\mathcal{G} \tag{A10}$$

$$P_{\text{e},g}^t - P_{\text{e},g}^{t-1} \leq \text{R}_{\text{e},g}^{60+} u_{\text{e},g}^{t-1}\Delta t + \alpha_{\text{e},g}^t \text{SU}_{\text{e},g}, \forall t\in\mathcal{T}, g\in\mathcal{G} \tag{A11}$$

$$P_{\text{e},g}^{t-1} - P_{\text{e},g}^t \leq \text{R}_{\text{e},g}^{60-} u_{\text{e},g}^t\Delta t + \beta_{\text{e},g}^t \text{SD}_{\text{e},g}, \forall t\in\mathcal{T}, g\in\mathcal{G} \tag{A12}$$

$$\sum_{g\in\mathcal{G}_j} P_{\text{e},g}^t + \sum_{k\in\delta_{\text{e},j}^+} P_{\text{e},k}^t - \sum_{k\in\delta_{\text{e},j}^-} P_{\text{e},k}^t = P_{\text{ed},j}^t + \sum_{c\in\mathcal{E}_{\text{gc},j}} P_{\text{ge},c}^t, \forall t\in\mathcal{T}, j\in\mathcal{N}_{\text{e}} \tag{A13}$$

$$P_{\text{e},k}^t - B_{\text{e},k}\left(\theta_{\text{e},k}^{+,t} - \theta_{\text{e},k}^{-,t}\right) = 0, \forall t\in\mathcal{T}, e\in\mathcal{E}_{\text{e}} \tag{A14}$$

$$P_{\text{e},k}^{\min} \leq P_{\text{e},k}^t \leq P_{\text{e},k}^{\max}, \forall t\in\mathcal{T}, e\in\mathcal{E}_{\text{e}} \tag{A15}$$

$$\sum_{g\in\mathcal{G}} R_{e,g}^t \geq \delta\sum_{j\in\mathcal{N}_{\text{e}}} P_{\text{ed},j}^t, \forall t\in\mathcal{T} \tag{A16}$$

where UT_g (h) and DT_g (h) are minimum up and down time of generator g, respectively. $\mathrm{UT_r}$ and $\mathrm{DT_r}$ (h) are remaining up and down time of generator g, respectively. δ (%) is the reserve requirement. $\mathrm{SU}_{\mathrm{e},g}$ (MW) and $\mathrm{SD}_{\mathrm{e},g}$ (MW) are start-up and shut-down ramp limit of generator g, respectively. $\mathrm{R}_{\mathrm{e},g}^{10+}$ (MW·h^{-1}) is the ramp up limitation within 10 minutes of generator g.

(A4) is the status transition of generators. (A5)–(A7) are the minimal up, down time duration, and initial status constraint of generators [33]. (A8)–(A10) are the power capacity limitation with reserves [33], [34]. (A11)–(A12) are the ramp up and down limitation [34]. The power balance of each bus is given in (A13), together with the compressor horse power. The power transmitted on each line is given in (A14), and the power is limited by (A15). Considering the uncertainty of load forecasting, the reserve requirement is given in Eq.(A16).

2) Gas System: The constraints of gas sources, pipelines, compressors and gas flow are formulated as follows:

$$Q_{\mathrm{g},s}^{\min} \le Q_{\mathrm{g},s}^{t} \le Q_{\mathrm{g},s}^{\max},\ \forall t \in \mathcal{T}, s \in \mathcal{S} \tag{A17}$$

$$L_{\mathrm{g},k}\left((V_{\mathrm{g},k}^{+,t}+V_{\mathrm{g},k}^{-,t})-(V_{\mathrm{g},k}^{+,t\text{-}1}+V_{\mathrm{g},k}^{-,t\text{-}1})\right) = 2\Delta t C_{1,k}(Q_{\mathrm{g},k}^{-,t}-Q_{\mathrm{g},k}^{+,t}),\ \forall t \in \mathcal{T}, k \in \mathcal{E}_{\mathrm{gp}} \tag{A18}$$

$$\frac{1}{4}L_{\mathrm{g},k}C_{2,k}(Q_{\mathrm{g},k}^{-,t}+Q_{\mathrm{g},k}^{+,t})\left|Q_{\mathrm{g},k}^{-,t}+Q_{\mathrm{g},k}^{+,t}\right| = \left(V_{\mathrm{g},k}^{+,t}\right)^2-\left(V_{\mathrm{g},k}^{-,t}\right)^2,\ \forall t \in \mathcal{T}, k \in \mathcal{E}_{\mathrm{gp}} \tag{A19}$$

$$-Q_{\mathrm{g},k}^{\max} \le Q_{\mathrm{g},k}^{+,t} \le Q_{\mathrm{g},k}^{\max},\ \forall t \in \mathcal{T}, k \in \mathcal{E}_{\mathrm{gp}} \tag{A20}$$

$$-Q_{\mathrm{g},k}^{\max} \le Q_{\mathrm{g},k}^{-,t} \le Q_{\mathrm{g},k}^{\max},\ \forall t \in \mathcal{T}, k \in \mathcal{E}_{\mathrm{gp}} \tag{A21}$$

$$V_{\mathrm{g},c}^{+,t} = R_{\mathrm{g},c}^{t}V_{\mathrm{g},c}^{-,t}, \forall t \in \mathcal{T}, c \in \mathcal{E}_{\mathrm{gc}} \tag{A22}$$

$$HP_{\mathrm{g},c}^{t} = \frac{a_{\mathrm{hp}}V_{\mathrm{sc}}Tq_{\mathrm{g},c}^{t}c_{\mathrm{k}}}{T_{\mathrm{sc}}\eta_{\mathrm{g},c}\,(c_{\mathrm{k}}-1)}\left(\left(R_{\mathrm{g},c}^{t}\right)^{\frac{c_{\mathrm{k}}-1}{c_{\mathrm{k}}}}-1\right), \forall t \in \mathcal{T}, c \in \mathcal{E}_{\mathrm{gc}} \tag{A23}$$

$$0 \le HP_{\mathrm{g},c}^{t} \le HP_{\mathrm{g},c}^{\max},\ \forall t \in \mathcal{T}, c \in \mathcal{E}_{\mathrm{gc}} \tag{A24}$$

$$V_{\mathrm{g},j}^{\min} \le V_{\mathrm{g},j}^{t} \le V_{\mathrm{g},j}^{\max},\ \forall t \in \mathcal{T},\ j \in \mathcal{N}_{\mathrm{g}} \tag{A25}$$

$$\sum_{s\in\mathcal{S}_j}Q_{\mathrm{g},s}^{t}+\sum_{k\in\delta_{\mathrm{g},j}^{+}}Q_{\mathrm{g},k}^{+,t}-\sum_{k\in\delta_{\mathrm{g},j}^{-}}Q_{\mathrm{g},k}^{-,t}+\sum_{c\in\mathcal{C}_{\mathrm{g},j}^{+}}Q_{\mathrm{g},c}^{t}-\sum_{c\in\mathcal{C}_{\mathrm{g},j}^{-}}Q_{\mathrm{g},c}^{t} = Q_{\mathrm{gd},j}^{t}+\sum_{g\in\mathcal{G}_{\mathrm{eg},j}}Q_{\mathrm{eg},g}^{t},\ \forall t \in \mathcal{T}, j \in \mathcal{N}_{\mathrm{g}} \tag{A26}$$

$$Q_{\mathrm{eg},g}^{t} = C_{\mathrm{g2e},g}\eta_{\mathrm{g2e},g}P_{\mathrm{e},g}^{t}, \forall t \in \mathcal{T},\ g \in \mathcal{G}_{\mathrm{eg}} \tag{A27}$$

$$P_{\mathrm{ge},c}^{t} = \eta_{\mathrm{e2g},c}HP_{\mathrm{g},c}^{t},\ \forall t \in \mathcal{T}, c \in \mathcal{E}_{\mathrm{gc}} \tag{A28}$$

The capacity bounds of each gas sources are depicted by Eq.(A17). The dynamic gas flow in a pipeline k is illustrated in Eq.(A18)–(A19). The volume flow rate is limited by Eq.(A20)–(A21). For the compressor, the pressure ratio and horsepower are given in Eq.(A22) and (A23), respectively. The horsepower of each compressor is constrained by Eq.(A24). Within the gas networks, the pressure of each node is to operate within given range in Eq.(A25). Considering the consumption of gas turbines, the gas node balance equation in shown in Eq.(A26). The gas consumption of gas turbine and electricity consumption of compressors are given in Eq.(A27) and (A28), respectively.

C. Second-Stage Constraint Set

Without considering the failures within the gas systems, the second stage constraint set, i.e., $\mathbf{Y}$ includes the real-time scheduling of generators, power flow and load shedding after the realization of transmission line failures, as follows:

$$P_{\mathrm{e},g}^{t}-R_{\mathrm{e},g}^{t} \le p_{\mathrm{e},g}^{t} \le P_{\mathrm{e},g}^{t}+R_{\mathrm{e},g}^{t}, \forall t \in \mathcal{T}, g \in \mathcal{G} \tag{A29}$$

$$-\mathrm{R}_{\mathrm{e},g}^{60\text{-}}\Delta t \le p_{\mathrm{e},g}^{t}-p_{\mathrm{e},g}^{t-1} \le \mathrm{R}_{\mathrm{e},g}^{60+}\Delta t, \forall t \in \mathcal{T}, g \in \mathcal{G} \tag{A30}$$

$$(I_{\mathrm{e},k}-1)\,M \le p_{\mathrm{e},k}^{t}-B_{\mathrm{e},k}\left(\gamma_{\mathrm{e},k}^{+,t}-\gamma_{\mathrm{e},k}^{-,t}\right) \le (1-I_{\mathrm{e},k})\,M,\ \forall t \in \mathcal{T}, k \in \mathcal{E}_{\mathrm{e}} \tag{A31}$$

$$-I_{\mathrm{e},k}P_{\mathrm{e},k}^{\max} \le p_{\mathrm{e},k}^{t} \le I_{\mathrm{e},k}P_{\mathrm{e},k}^{\max},\ \forall t \in \mathcal{T}, k \in \mathcal{E}_{\mathrm{e}} \tag{A32}$$

$$P_{\mathrm{ed},j}^{t} \ge p_{\mathrm{elc},j}^{t} \ge 0,\ \forall t \in \mathcal{T}, j \in \mathcal{N}_{\mathrm{e}} \tag{A33}$$

$$\sum_{g\in\mathcal{G}_j}p_{\mathrm{e},g}^{t}+\sum_{k\in\delta_{\mathrm{e},j}^{+}}p_{\mathrm{e},k}^{t}-\sum_{k\in\delta_{\mathrm{e},j}^{-}}p_{\mathrm{e},k}^{t} = P_{\mathrm{ed},j}^{t}+\sum_{c\in\mathcal{E}_{\mathrm{gc},j}}P_{\mathrm{ge},c}^{t}-p_{\mathrm{elc},j}^{t},\ \forall t \in \mathcal{T}, j \in \mathcal{N}_{\mathrm{e}} \tag{A34}$$

The real-time generator output constraints are given in (A29)–(A30). Considering the operating status of transmission lines, the power transmitted on each line is limited by (A31)–(A32). For specific bus, the amount of load shedding is given in (A33). The real-time power balancing at each bus is depicted by (A34).

D. Uncertainty Set

Considering the impacts of hurricane on transmission lines [27], only the operating status of transmission lines is treated as the uncertainty factors. The uncertainty set, i.e., $\mathcal{U}$ is depicted as follows

$$\sum_{k\in\mathcal{E}_{\mathrm{e}}}I_{\mathrm{e},k} \ge |\mathcal{E}_{\mathrm{e}}|-K \tag{A35}$$

where $|\mathcal{E}_{\mathrm{e}}|$ is the number of power transmission lines.

E. Solution Methods

The formulated problem (A1) is a non-convex mixed-integer min-max-min optimization problem, due to the non-convexity of constraint (A19). There are different methods to convexify this constraint, and the incremental piece-wise linear method [28] is adopted in this paper. $\mathbf{X}$ is reformulated to $\bar{\mathbf{X}}$, where constraint (A19) is piece-wise linearized, as follows

$$\min_{\mathbf{x}\in\bar{\mathbf{X}}} f(\mathbf{x})+\max_{\boldsymbol{\xi}\in\mathcal{U}}[\mathcal{Q}(\mathbf{x},\boldsymbol{\xi})] \tag{A36}$$

Problem is a standard two-stage robust optimization problem. In problem (A36), $\max_{\boldsymbol{\xi}\in\mathcal{U}}[\mathcal{Q}(\mathbf{x},\boldsymbol{\xi})]$ is a max-min problem, and the inner problem is a linear programming problem. The column-and-constraint generation method [35] is adopted to solve this problem. It should be noted that, the dual approach is adopted to solve $\max_{\boldsymbol{\xi}\in\mathcal{U}}[\mathcal{Q}(\mathbf{x},\boldsymbol{\xi})]$, while in [35] it is solved by a primal problem.

The formulated problem (A1)–(A36) is implemented after the close of day-ahead market, e.g., at 10:30 for PJM [36] before the operating day. The updated hurricane information and load forecasting information are input for the day-ahead two-stage robust UC problem. After the of day-ahead results are posted and before the close of rebid, e.g., 13:30 to 14:15 for PJM the commitment status of generators before the assessment period are determined and input to minimize the load shedding, as shown in (25) in Section IV, Part A. Due to the line failures, some committed generators might be shut down to meet the power balance and security requirements.

REFERENCES

[1] OECD(2018), "Outlook for natural gas," in *World Energy Outlook*. Paris: OECD Publishing, 2018, pp. 171–214. [Online]. Available: https://www.oecd-ilibrary.org/energy/world-energy-outlook-2018/outlook-for-natural-gas_weo-2018-7-en

[2] N. Judson, "Interdependence of the electricity generation system and the natural gas system and implications for energy security," Massachusetts Inst of Tech Lexington Lincoln Lab, Tech. Rep., Lexington, Massachusetts, United States, 2013, Art. no. 02420.

[3] I. G. Sardou, M. E. Khodayar, and M. Ameli, "Coordinated operation of natural gas and electricity networks with microgrid aggregators," *IEEE Trans. Smart Grid*, vol. 9, no. 1, pp. 199–210, Jan. 2018.

[4] J. Yang, N. Zhang, C. Kang, and Q. Xia, "Effect of natural gas flow dynamics in robust generation scheduling under wind uncertainty," *IEEE Trans. Power Syst.*, vol. 33, no. 2, pp. 2087–2097, Mar. 2018.

[5] U.S. Department of Energy, "Comparing the Impacts of the 2005 and 2008 Hurricanes on U.S. Energy Infrastructure," Tech. Rep., Washington, DC, United States, 2005, Art. no. 20585.

[6] J. Tang and H. R. Heinimann, "Quantitative evaluation of consecutive resilience cycles in stock market performance: A systems-oriented approach," vol. 532, Oct. 2019, Art. no. 121794.

[7] R. Billinton and G. Singh, "Application of adverse and extreme adverse weather: Modelling in transmission and distribution system reliability evaluation," *IEE Proc. Gener. Transm. Distrib.*, vol. 153, no. 1, pp. 115–120, 2006.

[8] R. Billinton and W. Li, *Reliability Assessment of Electric Power Systems Using Monte Carlo Methods*. Boston, MA: Springer US, 1994.

[9] Y. Zhou, A. Pahwa, and S.-S. Yang, "Modeling weather-related failures of overhead distribution lines," *IEEE Trans. Power Syst.*, vol. 21, no. 4, pp. 1683–1690, Nov. 2006.

[10] G. Li *et al.*, "Risk analysis for distribution systems in the northeast U.S. under wind storms," *IEEE Trans. Power Syst.*, vol. 29, no. 2, pp. 889–898, Mar. 2014.

[11] A. Hamada and A. El Damatty, "Failure analysis of guyed transmission lines during F2 tornado event," *Eng. Struct.*, vol. 85, pp. 11–25, 2015.

[12] X. Fu and H.-N. Li, "Uncertainty analysis of the strength capacity and failure path for a transmission tower under a wind load," *J. Wind Eng. Ind. Aerodyn.*, vol. 173, pp. 147–155, 2018.

[13] M. Panteli and P. Mancarella, "Modeling and evaluating the resilience of critical electrical power infrastructure to extreme weather events," *IEEE Syst. J.*, vol. 11, no. 3, pp. 1733–1742, Sep. 2017.

[14] M. Bessani *et al.*, "Probabilistic assessment of power distribution systems resilience under extreme weather," *IEEE Syst. J.*, vol. 13, no. 2, pp. 1747–1756, Jun. 2019.

[15] M. Panteli, P. Mancarella, D. N. Trakas, E. Kyriakides, and N. D. Hatziargyriou, "Metrics and quantification of operational and infrastructure resilience in power systems," *IEEE Trans. Power Syst.*, vol. 32, no. 6, pp. 4732–4742, Nov. 2017.

[16] S. Chanda and A. K. Srivastava, "Defining and enabling resiliency of electric distribution systems with multiple microgrids," *IEEE Trans. Smart Grid*, vol. 7, no. 6, pp. 2859–2868, Nov. 2016.

[17] S. Ma, B. Chen, and Z. Wang, "Resilience enhancement strategy for distribution systems under extreme weather events," *IEEE Trans. Smart Grid*, vol. 9, no. 2, pp. 1442–1451, Mar. 2018.

[18] G. Huang, J. Wang, C. Chen, J. Qi, and C. Guo, "Integration of preventive and emergency responses for power grid resilience enhancement," *IEEE Trans. Power Syst.*, vol. 32, no. 6, pp. 4451–4463, Nov. 2017.

[19] C. He, L. Wu, T. Liu, and Z. Bie, "Robust co-optimization planning of interdependent electricity and natural gas systems with a joint n-1 and probabilistic reliability criterion," *IEEE Trans. Power Syst.*, vol. 33, no. 2, pp. 2140–2154, Mar. 2018.

[20] J. Fang, Q. Zeng, X. Ai, Z. Chen, and J. Wen, "Dynamic optimal energy flow in the integrated natural gas and electrical power systems," *IEEE Trans. Sustain. Energy*, vol. 9, no. 1, pp. 188–198, Jan. 2018.

[21] M. H. Amirioun, F. Aminifar, S. Member, and M. Shahidehpour, "Resilience-promoting proactive scheduling against hurricanes in multiple energy carrier microgrids," *IEEE Trans. Power Syst.*, vol. 34, no. 3, pp. 2160–2168, May 2019.

[22] M. Shahidehpour, F. Wen, Y. Li, and Z. Li, "Minimax-Regret robust co-optimization for enhancing the resilience of integrated power distribution and natural gas system," *IEEE Trans. Sustain. Energy*, vol. 11, no. 1, pp. 61–71, Jan. 2020.

[23] X. Fu, H.-N. Li, and G. Li, "Fragility analysis and estimation of collapse status for transmission tower subjected to wind and rain loads," *Struct. Saf.*, vol. 58, pp. 1–10, 2016.

[24] M. Ouyang and L. D.-Osorio, "Multi-dimensional hurricane resilience assessment of electric power systems," *Struct. Saf.*, vol. 48, pp. 15–24, 2014.

[25] F. Xiao, J. D. McCalley, Y. Ou, J. Adams, and S. Myers, "Contingency probability estimation using weather and geographical data for on-line security assessment," in *Proc. IEEE Int. Conf. Probabilistic Methods Appl. Power Syst.*, 2006, pp. 1–7.

[26] Y. Liu and C. Singh, "A methodology for evaluation of hurricane impact on composite power system reliability," *IEEE Trans. Power Syst.*, vol. 26, no. 1, pp. 145–152, Feb. 2011.

[27] H. Zhang, L. Cheng, S. Yao, T. Zhao, and P. Wang, "Spatial-temporal reliability and damage assessment of transmission networks under hurricanes," *IEEE Trans. Smart Grid* vol. 11, no.2, pp.1044–1054, Mar. 2020.

[28] C. M. Correa-posada, and P. Sánchez-martín, "Gas network optimization: A comparison of piecewise linear models," *Optim. Online*, pp. 133–159, 2014.

[29] "Gurobi. (2020). Gurobi - The fastest solver - Gurobi," [Online]. Available: http://www.gurobi.com, Accessed on: Feb. 22, 2020.

[30] K. Alvehag and L. Soder, "A reliability model for distribution systems incorporating seasonal variations in severe weather," *IEEE Trans. Power Del.*, vol. 26, no. 2, pp. 910–919, Apr. 2011.

[31] K. Pambour, B. C. Erdener, R. B.-Lavin and G. Dijkema, "Development of a simulation framework for analyzing security of supply in integrated gas and electric power systems," *Appl. Sci.*, vol. 7, no. 1, 2017, Art. no. 47.

[32] P. M. Subcommittee, Probability subcommittee, "IEEE Reliability Test System," *IEEE Trans. Power Appar. Syst.*, vol. PAS-98, no. 6, pp. 2047–2054, Nov. 1979.

[33] G. M.-España, J. M. Latorre, and A. Ramos, "Tight and compact milp formulation of start-up and shut-down ramping in unit commitment," *IEEE Trans. Power Syst.*, vol. 28, no. 2, pp. 1288–1296, May 2013.

[34] N. Li, C. Uckun, E. M. Constantinescu, J. R. Birge, K. W. Hedman, and A. Botterud, "Flexible operation of batteries in power system scheduling with renewable energy," *IEEE Trans. Sustain. Energy*, vol. 7, no. 2, pp. 685–696, Apr. 2016.

[35] B. Zeng and L. Zhao, "Solving two-stage robust optimization problems using a column-and-constraint generation method," *Oper. Res. Lett.*, vol. 41, no. 5, pp. 457–461, 2013.

[36] J. Ciabattoni, "Commitment Process & Uplift Drivers," Tech. Rep., Valley Forge, Pennsylvania, United States, 2017, Art. no. 19460. [Online]. Available: https://www.pjm.com/-/media/committees-groups/committees/mic/20170224-special/20170224-item-04-commitment-process-and-uplift-drivers.ashx

Huajun Zhang (Student Member, IEEE) received the B.Eng. and M.Eng. degrees in electrical engineering from Shandong University, Jinan, China, in 2008 and 2011, respectively. She is currently working toward the Ph.D. degree with the Interdisciplinary Graduate School, Nanyang Technological University, Singapore. Her research interests include reliability and resilience evaluation of multi-energy systems on natural disasters, e.g., hurricanes.

Peng Wang (Fellow, IEEE) received the B.Sc. degree in electronic engineering from Xian Jiaotong University, Xian, China, in 1978, the M.Sc. degree from the Taiyuan University of Technology, Taiyuan, China, in 1987, and the M.Sc. and Ph.D. degrees in electrical engineering from the University of Saskatchewan, Saskatoon, SK, Canada, in 1995 and 1998, respectively. He is currently a Professor with the School of Electrical and Electronic Engineering, Nanyang Technological University, Singapore.

Shuhan Yao (Student Member, IEEE) received the B.Eng. degree in electrical engineering from Chongqing University, Chongqing, China, in 2013. He is currently working toward the Ph.D. degree with the Interdisciplinary Graduate School, Nanyang Technological University, Singapore. His research interests include smart grid resilience, optimization and reinforcement learning.

Xiaochuan Liu (Student Member, IEEE) received the B.Eng. degree in electrical engineering from Wuhan University, Wuhan, China, in 2015, and the M.Sc. degree from Nanyang Technological University, Singapore, in 2016. He is currently working toward the Ph.D. degree with the School of Electrical and Electronic Engineering, Nanyang Technological University, Singapore. His research interests include applied optimization and power system operation.

Tianyang Zhao (Member, IEEE) received the B.E., M.E., and Ph.D. degrees in electrical engineering from North China Electric Power University, Beijing, China, in 2011, 2013, and 2017, respectively. He is currently a Postdoctoral Research Fellow with the Energy Research Institute, Nanyang Technological University, Singapore. His research interests include power system operation optimization, resilience and game theory.